Structure of the Ice Nanocrystal Surface from Simulated versus Experimental Spectra of Adsorbed CF4

ARTICLE *in* THE JOURNAL OF PHYSICAL CHEMISTRY · FEBRUARY 1996

Impact Factor: 2.78 · DOI: 10.1021/jp952193w

4 AUTHORS, INCLUDING:

J. Paul Devlin
Oklahoma State University - Stillwater
203 PUBLICATIONS **5,517** CITATIONS

Structure of the Ice Nanocrystal Surface from Simulated versus Experimental Spectra of Adsorbed CF_4

V. Buch*

Department of Physical Chemistry and the Fritz Haber Research Center, The Hebrew University, Jerusalem 91904, Israel

L. Delzeit, C. Blackledge, and J. P. Devlin

Department of Chemistry, Oklahoma State University, Stillwater, Oklahoma 74078

Received: August 1, 1995; In Final Form: November 8, 1995[⊗]

CF_4 adsorbate uptake and spectra are simulated on various model icy surfaces and compared to experimental data measured for CF_4 adsorbate on ice nanocrystals. Comparison suggests that surfaces of annealed ice nanocrystals are relatively smooth but laterally disordered, while surfaces of unannealed nanocrystals are disordered and rough. CF_4 adsorbate structure and uptake display remarkable sensitivity to the structural features of the ice surface models and in particular to the extent of disorder. Asymmetric CF stretch spectroscopy of CF_4 adsorbate is suggested as a useful probe of the surface structure of molecular solids and of large molecular clusters.

I. Introduction

Gas adsorption on icy surfaces is of interest in terrestrial, atmospheric, and interstellar chemistry.[1] The present study was carried out in the framework of our research program to investigate structure and spectroscopy of icy surfaces and of adsorbates on ice.[2−6] In this study, the hydrophobic CF_4 adsorbate is considered. Grand canonical Monte Carlo (GCMC) simulations were carried out of the uptake and the structure of the adsorbate on icy surfaces. CF_4 spectra were calculated and compared to experiment. To facilitate the interpretation, additional calculations of CF_4 spectra were carried out for various assumed (ordered and disordered) model structures of the adsorbate layer. One of the aims was to investigate the interaction of a small hydrophobic molecule with the icy surface. The issues addressed included surface binding sites favored by the adsorbate, the extent of clustering of adsorbate molecules on the surface, and the interplay between adsorbate structure and spectroscopy. Perhaps the most interesting finding of the present study is the marked sensitivity of the adsorbate uptake and spectroscopy to the molecular structure of the underlying ice surface. We then used CF_4 adsorbate spectroscopy as an aid to characterize icy surfaces.

The current molecular level understanding of the surface structure of water ice is much more limited than that of the ice interior. Among recent studies of ice surface properties, one may note a low-energy electron diffraction (LEED) study of an ice film,[7] simulations of structure and dynamics of crystalline[8] and amorphous[6] ice surfaces, studies of the relation between the ice surface structure and its infrared spectroscopy,[3,4] and computational modeling of the ice−liquid interface.[9] A considerable body of literature is also available on H_2O adsorption on metals.[10]

In the present study we address molecular surface structure of ice *nanocrystals*. Recently, Devlin et al.[3,4] developed an experimental technique to prepare stable deposits of such nanocrystals, of a very large surface area with respect to gas adsorption; the deposits proved to be useful in experimental investigations of the ice surface spectroscopy and of gas−ice surface interactions.[3,4] Here, the CF_4 adsorbate spectroscopy is used to probe the nanocrystal surfaces. One lesson which we learned from these studies is that the crystalline interior of the nanocrystals (evidenced clearly by their infrared spectra) does not imply an ordered surface structure.

The observable of the present interest is the vibrational fundamental of the triply degenerate ν_3 asymmetric CF stretch of CF_4. This vibration is characterized by a very large direction independent dipole derivative,[11] and therefore oscillations of neighboring CF_4 molecules are strongly coupled to each other by the dipole−dipole interaction. Infrared spectra of condensed phases of CF_4 are dominated by *collective in-phase* vibrations. The spectra of solid films of CF_4 were shown by Jones and Swanson[11] to display two prominent features at 1235 and 1337 cm^{-1}, due to transverse optical (TO) and longitudinal optical (LO) vibrations, where the TO (LO) excitation corresponds to the in-phase vibration of CF_4 polarized in the direction parallel (perpendicular) to the film.[12] A discussion of LO-TO splitting in films of crystalline and amorphous molecular solids can be found, e.g., in refs 12a−f. Recently, Rowland, Kadagathur, and Devlin[5] showed that a similar LO−TO splitting pattern appears in the vibrational spectrum of CF_4 adsorbate on ice nanocrystals at about a monolayer coverage, with splitting reduced to ∼75 cm^{-1}. As the CF_4 coverage of the nanocrystal surfaces is reduced, the LO−TO splitting gradually decreases toward a single peak, indicating transition from a continuous adsorbate layer toward isolated adsorbate molecules and/or small adsorbate clusters. In the present study, additional CF_4 spectra are presented on ice nanocrystals prepared under different experimental conditions, on glassy and crystalline particles of trimethylbenzene (mesitylene), and on CO_2 nanocrystals. We exploit the structural sensitivity of the CF_4 adsorbate spectra (which is due to strong intermolecular coupling between CF_4 vibrations) to probe surface properties of the different nanoparticles.

The article is organized as follows: Section II describes the experiments. Section III is devoted to computational modeling of CF_4 adsorbate. In section IV we interpret the experimental data, using the results of the modeling. Summary and concluding remarks are presented in section V.

[⊗] Abstract published in *Advance ACS Abstracts,* January 15, 1996.

0022-3654/96/20100-3732$12.00/0

II. Experiment

A. Experimental Methods. As reported in more detail elsewhere,[4,5] our studies of ice nanocrystals are based on their formation in the gas phase following the rapid expansion of a ~1% mixture of $H_2O(D_2O)$ in N_2(g) or He(g) into a precooled cluster cell to static pressures of $^1/_4$−$^1/_2$ atm at cell temperatures ranging from 70 to 90 K. In the present study, in addition to cubic ice nanocrystals, nanoparticle samples of symmetrical trimethylbenzene (mesitylene) have been similarly prepared at 100 K, and nanocrystals of CO_2 have been formed in helium−CO_2 mixtures at 50 K. The cylindrical cluster cell, the inner part of a double-walled vacuum chamber, has thick brass walls and zinc sulfide end plates sealed with indium gaskets. The larger version of this cell is 5 cm in diameter and 15 cm in length while a smaller version is 1.5 × 3 cm. The cells are cooled by connection to the stem of an APD closed-cycle helium refrigerator.

Spectra are measured of deposits formed by the attachment of a few percent of the gas-phase nanoparticles to the infrared-transparent end windows of the cell. The optical thickness of the network of suspended particles is limited only by the number of separate load−pump cycles used to form the deposits. The ice nanocrystalline samples, with approximately 10% of the water molecules on the surface, are stable indefinitely at temperatures below 110 K. From the band intensity of the dangling H (D) surface-localized stretching vibration,[2] the average particle size of a fresh deposit of cubic ice is estimated as 20 nm. From the induced shifting of this band, it is clear that volatile adsorbates have full access to the particle surfaces.

Particularly advantageous to the present study is our ability to (a) anneal the nanoparticles to influence particle surface characteristics and particle phases and (b) choose optimum sample temperatures and adsorbate pressures. For example, amorphous mesitylene nanoparticles, deposited at 100 K, crystallize upon annealing at 140 K (as indicated by a pronounced sharpening of the mesitylene particle infrared bands). Spectra of adsorbed CF_4 have been measured on the ice and mesitylene particles at 83 K and pressures ranging from 0.01 to 0.06 Torr and also on a vapor deposite of microporous amorphous ice for the same temperature and CF_4 pressure range. The accuracy of the pressure (P) determination is several percent in the high-pressure limit, but the uncertainty in P increases to about 30% at 0.01 Torr. At the sampling temperature (83 K) a section of the cell wall near the refrigerator cold stem, also coated with nanoparticles, is slightly cooler than the windows which support the samples. These colder adsorbent particles limit the CF_4 vapor pressure to ~0.14 Torr, which, in turn, limits the sample CF_4 coverage to a monolayer or less.

More specifically, the CF_4 adsorbate spectra have been obtained for fresh ice nanoparticle deposits in both cell types, nanoparticles annealed at 140 K within the larger cell, microporous amorphous ice vapor deposits, crystalline and amorphous mesitylene nanoparticles, and CO_2 nanocrystals at pressures ranging from 0.01 to 0.1 Torr; particular attention is given to the band complex of the CF_4 antisymmetric stretching mode for which the gas-phase frequency is 1283 cm^{-1}. As in previous ice adsorbate studies,[4] the position of the surface dangling H vibration has been routinely monitored as a secondary measure of adsorbate surface coverage. The spectra have been obtained using either a Bio-Rad FTS-20 or a FTS-40 spectrometer at a nominal resolution of 4 cm^{-1} and scan counts of typically 400.

B. Experimental Results. The emphasis here is on the marked dependence of the spectrum of adsorbed CF_4 on the nautre of the nanoparticles and their surfaces and with the extent of coverage as controlled by the gas overpressure, the intent being to note patterns in the behavior of the spectra. Since the data for CF_4 adsorbed on the ice surfaces are for annealed and unannealed nanoparticles prepared in two different cell types, the question arises as to the relative crystallinity of the ice that underlies the different surfaces. For that reason the crystalline/amorphous nature of the interior ice for the different classes of samples will be examined before considering spectra of the adsorbed CF_4.

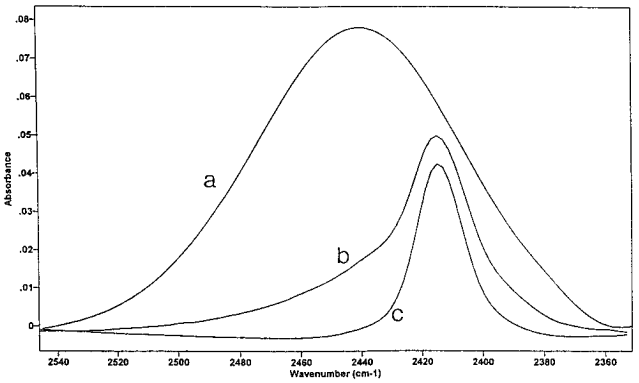

Figure 1. O−D stretch band for a few percent HOD isolated/decoupled within different H_2O ices: (a) microporous amorphous ice, (b) ice nanoparticles freshly prepared in the small cluster cell, and (c) ice nanoparticles prepared and annealed at 140 K in the larger cluster cell. Spectra were obtained at ~83 K.

1. Ice Crystallinity from the O−D Stretch of Decoupled HOD. Because the full width at half-maximum (fwhm) of the band of the O−D stretch mode for a few percent of HOD isolated in H_2O ice is known to decrease dramatically, from ~80 to near 20 cm^{-1}, during crystallization of amorphous ice, this band is an effective indicator of the degree of crystallinity of ice samples in general and of our ice nanoparticles in particular. Thus, the O−D stretch-mode bands presented in Figure 1 indicate the degree of crystallinity of the classes of ice samples of interest here. From top to bottom, typical curves are shown for three different classes of ice samples: amorphous ice films, fresh nanoparticles prepared in the small cluster cell, and nanocrystals prepared in the larger cell and annealed at 140 K.

The obvious conclusions from comparison of the curves of Figure 1 are that the ice nanoparticles prepared in the larger cluster cell (whether annealed or not) are dominantly crystalline (curve c) while the fresh particles prepared in the smaller cell contain a significant amorphous component (curve b). The particles formed in the two cells are of similar average size, so the amorphous component of the small-cell particles apparently reflects a more rapid cooling of the gas-phase nanodroplets caused by the proximity of the cold walls. It is known that the clusters form within a centimeter of the orifice of the delivery tube of the gaseous mixture,[2k] a distance similar to the diameter of the small cluster cell.

On the scale used to display the O−D stretch band in Figure 1, neither the spectra of ice particles freshly prepared in the larger cell nor those of particles subsequently annealed at 120 K are distinguishable from curve c (of the 140 K-annealed nanocrystals) and, therefore, are not included. However, more sensitive comparisons of spectra do reflect some more subtle effects. For example, the HOD band, such as in Figure 1c, can be resolved into the band of the interior crystalline HOD molecules with the fwhm of 20 cm^{-1} and a broader underlying band (~70 cm^{-1} fwhm) having approximately the same peak position. The latter component is expected to originate from OD bonds participating in distorted hydrogen bonds in a more

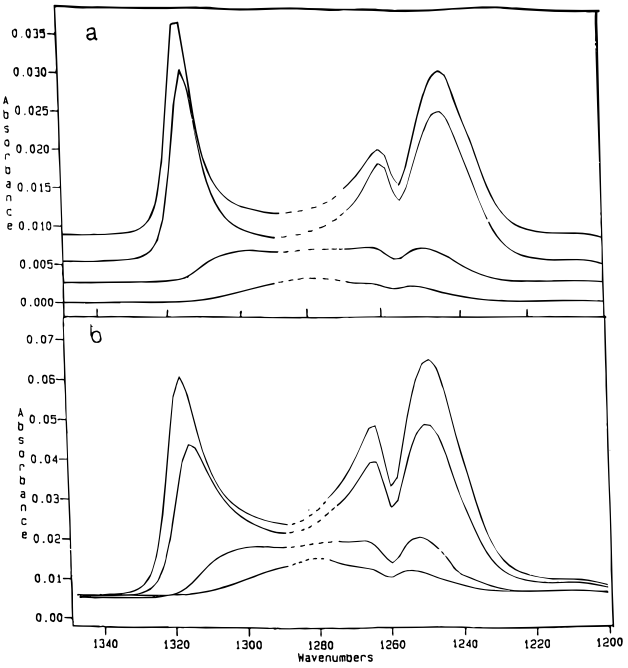

Figure 2. Infrared band complex of the antisymmetric stretch mode of adsorbed CF_4 at 83 K: from top to bottom of each series the CF_4(g) pressures were 0.06, 0.04, 0.02, and 0.01 Torr. The labels denote ice nanoparticles formed in the large cell and (a) annealed at 140 K and (b) scanned unannealed. Dashed line denotes location of the subtracted CF_4(g) band.

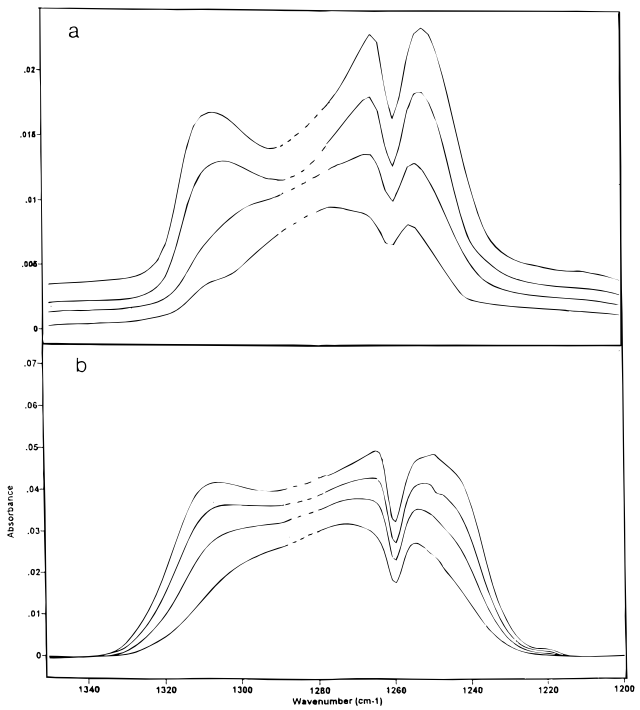

Figure 3. Same as Figure 2 except the labels denote (a) nanoparticles freshly prepared in the small cluster cell and (b) a vapor deposit of microporous amorphous ice.

disordered ice material. The intensity of this component is consistent with a few disordered surface layers of ice, if the broad contribution is assumed to originate from the nanocrystal surface material. We emphasize that the frequency of the broad contribution is *not* consistent with HDO isotopically diluted in *bulk amorphous ice* (see Figure 1a), which provides additional support for the surface assignment. Moreover, the broad component decreases during annealing roughly in proportion to the decrease in the surface area, as evidenced by the decrease in the intensity of the dangling OD (or OH) surface band. (The average particle size in the network of nanocrystals increases during annealing; see ref 4.)

2. Spectra of Surface-Adsorbed CF_4. The absorption pattern of the antisymmetric stretch mode of adsorbed CF_4 as a function of gas pressure at 83 K is presented in Figures 2 and 3 for the different classes of ice samples described above. As noted previously,[5] at pressures near 0.06 Torr these patterns are dominated by features assigned to the collective transverse ($\sim$1250 cm^{-1}) and longitudinal ($\sim$1320 cm^{-1}) modes of the adsorbate layer, while at lower surface coverage the vibrations of individual decoupled CF_4 molecules (and/or of small groups of CF_4) give a single band centered near 1275 cm^{-1}. (The Evan's hole at 1260 cm^{-1} visible in all the spectra is due to a Fermi resonance with an overtone state corresponding to two quanta of CF_4 bending;[5] this hole will not be discussed in detail in the present study.) Though this is a general description of each of the series of spectra, there are obvious differences between the series, and relative to the series for the 140 K annealed ice in Figure 2a, these differences increase through the sequence Figure 2a−Figure 3b.

The variations in spectra for coverage corresponding to 0.06 Torr of CF_4 pressure, from Figure 2a to Figure 3b (i.e., in a series ranging from well-annealed nanocrystals to microporous amorphous ice), can be summarized as follows: the TO and LO peaks increase in breadth; the splitting between the TO and LO peaks decreases; more of the band intensity appears in the intermediate frequency range between LO and TO, near the decoupled mode frequency; the ratio of LO peak intensity to TO peak intensity decreases from greater than to significantly less than unity (the spectrum of CF_4 on amorphous ice (Figure 3b) is an exception in the last trend). Further, it is clear that the band intensity for the 0.01 Torr spectra, relative to that for 0.06 Torr, increases dramatically in this series.

These variations appear to be related to the degree of crystallinity of the sample for the various classes. But crystallinity is a macroscopic property of sample interior while the spectra of adsorbed CF_4 should relate to the microscopic properties of the ice surface. So perhaps it is not surprising that the spectra change measurably from Figure 2a to Figure 2b, even though each corresponds to CF_4 adsorbed on particles that have a crystalline interior. (Note that at 0.06 Torr the LO:TO peak intensity ratio is greater than 1 in Figure 2a and less than 1 in Figure 2b.) That these variations are not a simple reflection of the crystallinity of the nanoparticle interior is clear from comparison of CF_4 spectra on ice nanocrystals, to the corresponding series of spectra of CF_4 adsorbed on amorphous and crystalline mesitylene nanoparticles (Figure 4a,b). From comparison of Figure 2a to Figure 4 it is clear that CF_4 spectra on *annealed crystalline* ice nanoparticles evolve as a function of pressure in a manner similar to that of CF_4 on *glassy* rather than on crystalline mesitylene. In Figure 4a,b, significant differences are seen between the spectra of CF_4 adsorbed on amorphous and crystalline mesitylene nanoparticles. While the TO−LO splittings are similar for 0.10 Torr, the splitting for the "crystalline" surface is much less sensitive to reduced coverage, remaining relatively unchanged down to $\sim$0.4 of a monolayer at 0.035 Torr (not shown). As can be noted in Figure 4c, this insensitivity to coverage is also apparent for CO_2 nanocrystals for which the TO−LO splitting is nearly unchanged even at less than 33% coverage. Interpretation of these spectral patterns in terms of the structure of the adsorbate layer and of the underlying nanoparticle surface will be pursued in section IV.

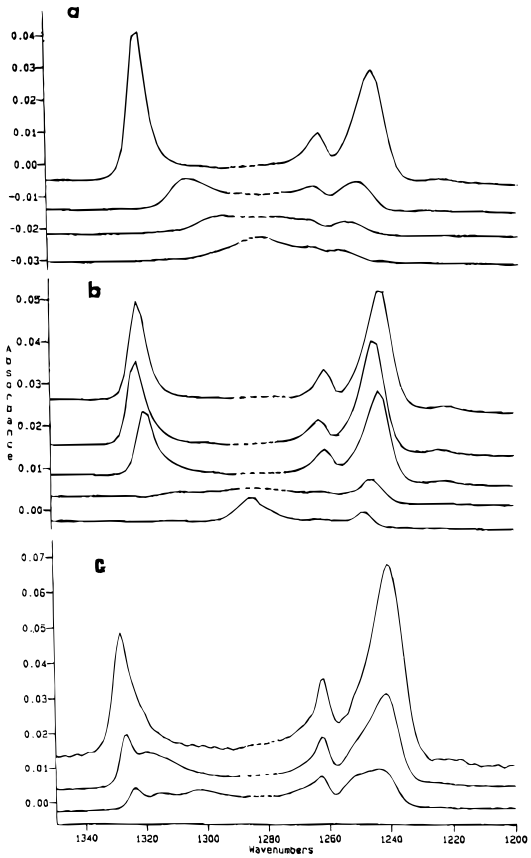

Figure 4. Infrared band complex of the antisymmetric stretch mode of CF_4 adsorbed on (a) amorphous nanoparticles of mesitylene at 83 K, $P[CF_4(g)] = 0.1$, 0.06, 0.04, and 0.02 Torr (top to bottom); (b) nanocrystals of mesitylene at 83 K, $P[CF_4(g)] = 0.1$, 0.08, 0.06, 0.04, and 0.02 Torr; and (c) CO_2 nanocrystals at 78 K, pressure range 0.04−0.01 Torr.

III. Computational Details

A. Calculation of Adsorbate Spectra. The antisymmetric stretch vibration of an isolated CF_4 molecule is triply degenerate. The vibrational Hamiltonian is given by $H_{vib} = \sum_{j,k} h^{\circ}_{j,k} + \sum_{j,k,j',k'} D_{jk,j'k'}$, where $h^{\circ}_{j,k}$ denotes a Hamiltonian of a harmonic oscillator localized on molecule J and oscillating in the direction k ($k = x$, y, or z). The intermolecular coupling $D_{jk,j'k'}$ between the oscillators is approximated as the dipole−dipole interaction.[12a,b] The dipole derivative with respect to the vibrational displacement, μ', is adopted from ref 11 as 0.596 $eu^{-1/2}$. This value, derived in ref 11 from the LO−TO splitting in solid CF_4 films, is within a few percent of the gas-phase value,[13] and thus condensation does not affect μ' significantly. To calculate vibrational states, we employ an exciton basis, i.e., a basis of products of harmonic eigenstates localized on the different molecular oscillators. The ground state is approximated as a product of harmonic ground states $|000...000\rangle$. A vibrationally excited state is approximated as a linear combination of single excitations: $\Psi_{exc} = \sum c_{jk} |000...1_{jk}...000\rangle$. (In each basis state all harmonic oscillators are in their ground states except the kth oscillator of molecule j, which in the first excited state.) The energies of Ψ_{exc} and the coefficients c_{jk} are calculated by diagonalization of the Hamiltonian matrix. The spectra are obtained by binning the intensities of transitions between the ground state and the excited states. The absorption intensity for incoming radiation polarized in the kth direction is calculated as the squared matrix elements of the oscillating dipole: $|\langle\Psi_0|\mu'\sum_j \delta q_{jk}|\Psi_{exc}\rangle|^2$. The resolution used in binning the spectra was (unless stated otherwise) 4 cm^{-1}, as in the experimental spectra shown in Figures 2−4.

Calculations of CF_4 spectra are carried out for model adsorbate layers of different structures, described in the following sections. Two-dimensional boundary conditions are employed in most of the calculations; that is, we generate CF_4 adsorbate structure for a square of rectangular patch of surface (of linear dimensions in the range 36−38 Å) and use a periodic "superlattice" of such patches in the calculation of the spectrum. The spectra are calculated for $K = 0$; i.e., the coefficient c_{jk} in Ψ_{exc} above is assumed the same for all copies of oscillator jk in all unit cells. The assumed "flat" model is of course an approximation; the nanocrystals are formed, most probably, via freezing of spherical liquid droplets, and their surfaces are likely to be curved. One of the results of a (presumably) spherical shape is that all directions of the radiation polarization with respect to the local normal to the nanocrystal surface are equally probable. To account for this fact, the spectra are averaged over all possible incoming radiation polarizations, with respect to the model patch of the nanocrystal surface.

Modeling of spectra of an entire CF_4 monolayer on a nanocrystal of the experimental size (∼20 nm diameter) is beyond our capabilities. Some test calculations were carried out however for CF_4 adsorbate on much smaller ice cluster models (several nanometers in diameter), for which direct evaluation of the spectra for the entire CF_4 adsorbate layer (without periodic boundaries) is feasible.

The coupling between CF asymmetric stretch fundamental and the bending overtone at 1260 cm^{-1} was neglected, and therefore the Evan's hole seen in the experimental spectra (Figures 2−4) is not reproduced by the present calculations.

B. Simulated Spectra of Random and Ordered CF_4 Layers. We now discuss several simple models for the adsorbate structure. That is, different (ordered and disordered) structures are assumed for the adsorbate, and the corresponding spectra are calculated. The objective is to identify qualitative factors affecting CF_4 line shapes near monolayer coverage.

1. Description of the Models. The model structures are described briefly below; more details can be found in the microfilm material. The model parameters were selected to cover roughly the range of the experimentally observed variations in the CF_4 spectra on ice at 0.06 Torr.

(a) Crystalline Monolayers. CF_4 molecules were arranged in the $x-y$ plane in a crystalline (hexagonal or cubic) pattern; the lateral nearest-neighbor distance was set to 4.25 Å.

(b) Random Flat Layers. These calculations were carried out to demonstrate the effect of structural disorder on the spectra. The CF_4 structure used to generate the spectra was obtained by picking the adsorbate x,y coordinates at random within a large 37 × 37 Å "unit cell" (see section IIIA on periodic boundary conditions). The CF_4 z coordinates were picked from a Gaussian distribution of width 2σ in the range 1−6 Å. No two molecules were allowed within a distance of less than 4 Å (roughly the diameter of CF_4) from each other.

(c,d) Crystalline and Disordered CF_4 Shells. These models are analogous to models a and b above; however, the molecules are arranged in a spherical shell of mean radius of 24 Å, rather than in a flat layer.

2. Results. Figure 5a shows simulated spectra for a hexagonal and cubic crystalline arrangement of the CF_4 layer. The LO−TO splitting is larger for the cubic arrangement (due to larger density); however, the two crystal spectra are otherwise similar—a pair of sharp peaks is obtained in each case, with the TO integrated intensity twice that of the LO. The TO peak intensity is also larger than that of the LO.

The solid line in Figure 5b shows the effect of lateral disorder on the spectrum. The CF_4 molecules are now randomly

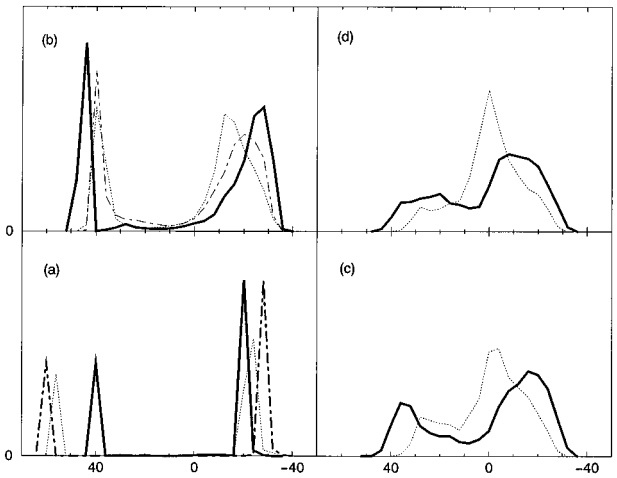

Figure 5. Spectra of model CF_4 layers and spherical shells of different properties. (a) Ordered CF_4: solid line, a crystalline hexagonal monolayer; dot-dashed, a simple cubic monolayer; dotted, an ordered CF_4 shell, a spherical analog to a 2D cubic crystal. (b−d) Spectra of disordered CF_4 layers (solid, dot-dashed lines) and of disordered CF_4 shells of mean diameter of 24 Å (dotted). The thicknesses of the layers and the shells are 1 Å (solid, b), 2 Å (dot-dashed, b), 0.5 Å (dotted, b), 4 Å (solid and dotted, c), and 6 Å (solid and dotted, d).

distributed within a thin layer. The main effect of disorder is very significant broadening of the TO peak. The TO integrated intensity is still twice that of the LO, but the TO peak is broadened significantly and LO only slightly, and therefore the LO peak intensity is now larger than that of the TO.[14]

Figures 5b−d shows the effect of adding vertical disorder to the lateral disorder in the adsorbate layer. Vertical disorder is represented by a random (Gaussian) distribution of the adsorbate *z* coordinates; the width of the distribution is now increased from 1 to 6 Å. This is a crude representation of the effect of making the underlying substrate surface rougher in a disordered fashion. Increase of 2σ from 1 to ∼3 Å reduces the LO−TO splitting, but the basic "narrow LO/broad TO" spectral pattern is retained. (The width of the adsorbate *z* distribution obtained in GCMC simulations on smooth icy surfaces is less than 3 Å; see next section.) However at $\Delta z \gtrsim 4$ Å, the spectrum is broadened significantly with respect to the "smooth" case. The LO and TO peaks are so broad that they merge in the middle, and considerable intensity builds up at the center, around the decoupled CF_4 frequency (see solid lines, Figure 5c,d). Because of broadening of *both* peaks, the TO peak intensity is again larger than that of the LO.

The range of behaviors displayed by the random layer models is qualitatively consistent with the changes occurring in the experimental CF_4 adsorbate spectra at 0.06 Torr, as the nanocrystals are annealed. Comparison between the experimental spectra shown in Figures 2 and 3 and the calculations of Figure 5 suggests that (a) surfaces of unannealed nanocrystals are both disordered and rough, (b) unannealed nanocrystals generated in small cells are much rougher than the ones generated in large cells, and (c) annealed nanocrystals have smooth but still laterally disordered surfaces.

A surface of a nanocrystal may be inhomogeneous; i.e., it may include structurally different patches on which the adsorbate distributions have different statistical (or nonstatistical) properties. To examine the effect of inhomogeneity, numerical experiments were carried out for random CF_4 layers of a "checkerboard" pattern, including patches of two distinct statistical properties. The resulting spectrum was not an average of the two spectra of the two respective models, but rather an intermediate spectrum. In particular, a checkerboard structure of two thin laterally disordered CF_4 patches of different thicknesses still resulted in a "sharp LO/broad TO" pattern, with intermediate peak frequencies. Thus, this characteristic spectral signature of a smooth laterally disordered surface allows for considerable inhomogeneity in surface properties.

We finally examine the effect of the surface curvature on the simulated spectra by comparing results for spherical shells of CF_4 with those for analogous flat layers. These tests were carried out since the experimental nanocrystals are likely to be spherical; however, to make the calculation feasible, the shell diameter used was about 4 times smaller than the typical nanocrystal diameter. The results for different shell thicknesses are shown in Figure 5 as dotted lines. The qualitative evolution of the spectra in Figure 5a−c from two narrow peaks of the ordered CF_4 shell toward a narrow LO/broad TO pattern for the disordered thin shell and two broad overlapping peaks for a 4 Å thick shell is similar to the horizontal layer results, although in shells the LO−TO splitting is smaller and LO broadening occurs at lower thicknesses. In the thickest shell spectrum (Figure 5d), the doubly peaked line shape collapses to a single peak with a shoulder; this qualitative difference with respect to the flat layer result is not surprising, considering that now the shell thickness is a significant fraction of the mean shell radius.

C. Grand Canonical Monte Carlo Simulations of Adsorbate Uptake and Spectra on Model Icy Surfaces. In this section we attempt to advance beyond the simple models of adsorbate structure described above toward molecular level understanding of the system. We shall address the question: What kind of icy surfaces support adsorbate structures with spectra consistent with the experiment? More generally, the objective is to investigate the mechanisms and the energetics of CF_4 adsorption on icy surfaces. As explained in section IIIA, the nanocrystals are too large to be simulated whole; we simulate instead adsorbate uptake on model patches of their surfaces. The patches are represented by ice slabs, with two-dimensional boundary conditions in the directions parallel to the surface. The molecular structure of the different surface models is shown in Figures 6 and 10 and discussed below in more detail.

1. Models of Nanocrystal Surfaces. The structure of crystalline ice formed at low pressures is either hexagonal or cubic; the former is the thermodynamically stable phase; however, the latter appears to be the kinetically preferred in fast freezing of small droplets and clusters.[15,16] The nanocrystals are most probably of the cubic ice structure, although the infrared OH stretch spectra used to determine the crystallinity are very similar for the two forms. The cubic and hexagonal structures are in many ways closely related.[17] Both correspond to a tetrahedral network of hydrogen bonds, and both can be viewed as containing H_2O layers composed of hexagonal rings; the two forms differ in the stacking arrangement of the layers. While the arrangement of the O atoms is crystalline, both forms of ice are proton-disordered; i.e., the disordered arrangement of the H atoms is restricted only by the so-called ice rules[18] (according to which one H atom is present between every pair of neighboring O atoms, and each O atom participates in two chemical bonds to H atoms).

However, crystallinity of the nanocrystal interior does not ensure crystallinity of the nanocrystal surfaces. The crystalline tetrahedral network of bonds is favorable for the bulk; however, it is not necessarily favorable for the surfaces. This is since a crystalline surface is associated with the presence of a large number of dangling atoms, i.e., H and O atoms of water molecules with unsaturated hydrogen bond coordination. It has been noted by Kroes in molecular dynamics simulations of the

(0001) surface of hexagonal ice[8] at 190 K that the surface relaxes while increasing the hydrogen bond coordination, at the expense of the lateral order of the O atoms. (Entropy may also drive the surface toward disorder, if a large number of nonperiodic low-energy configurations are available.) Surface disorder was also indicated by our studies of structure and spectra of the analogous (111) surface of cubic ice.[4] Moreover, the simple models of the previous section suggest that even the annealed nanocrystals are covered by disordered adsorbate monolayers, which in turn suggests disorder in the underlying top layer of the icy surface.

Additional experimental evidence appears consistent with disorder in the topmost layer(s) of ice, although it does not *prove* surface disorder. As discussed in section IIB1, a broad weak component of the OD stretch spectrum of HOD isotopically diluted in large-cell H_2O nanocrystals appears to originate from disordered ice surface material. Torchet et al.[15] and Huang and Bartell[16] reported electron diffraction patterns of ice clusters generated in jet expansion, albeit much smaller than the nanocrystals considered here, containing thousands rather than hundreds of thousands of water molecules; the diffraction patterns included a disordered component, possibly originating (at least partially) from a disordered surface layer. Moreover, Torchet et al. found[15] in their experiments that water clusters containing a few hundred molecules were amorphous. This result can be contrasted, e.g., with the results for CO_2 clusters, which retain cubic crystalline bulk structure down to the size of several tens of molecules. These findings suggest that the cubic crystalline structure is favored by the interior of the water clusters rather than by the surface, since the crystalline strucrure does not develop for clusters which are too small to have a significant fraction of interior molecules. (The same argument suggests that CO_2 cluster surfaces are crystalline; we shall return to this point in the discussion of CF_4 spectra on CO_2 nanocrystals.) Finally, a recent LEED study[7] of the surface of an ice film (most likely the (0001) surface of hexagonal ice) indicated disorder in the topmost ice layer; the authors proposed dynamical disorder, due to large-amplitude molecular oscillations, but did not rule out the possibility of static disorder.

If surface disorder is in fact present, a question arises concerning its origin. In the unannealed samples, the surface structure is determined by kinetics of processes associated with nanocrystal formation and deposition, rather than by the thermodynamic stability. This is recognized since annealing of these samples results in irreversible changes in surface structure evidenced by changes in the CF_4 adsorbate spectrum (Figures 2 and 3a). On the other hand, the surface structure of nanocrystals annealed at 140−150 K may approach that form which is most stable thermodynamically for cubic ice nanocrystals. (When we refer here to a thermodynamically stable surface structure, we mean that structure which corresponds to the lowest free energy, given the cubic ice interior. The cubic ice structure of clusters and small particles was argued by Bartell to be metastable.[16b]) To approach such a stable form, the surface water molecules must be able to rearrange in this temperature range. Amorphous ice (which is a totally disordered form of ice) undergoes a spontaneous transition to crystalline cubic ice at ∼145 K (on a time scale of ∼10 min). It is found experimentally that the interiors of initially poorly crystallized nanocrystals improve their crystallinity upon annealing at 130 K, as evidenced by changes in the infrared line shape of the bulk OD (or OH) stretch (see Figure 1 and section IIB1). It thus appears that the *surface* water molecules of nanocrystals should have enough freedom of motion to rearrange into a crystalline structure in the 140−150 K temperature range. If a crystalline form is not attained, then apparently the crystalline form is not preferred. (Of course, upon cooling back to 83 K the nanocrystal surface may freeze into a metastable form characteristic of some temperature between 140 and 83 K, rather than into a thermodynamically stable form characteristic of 83 K, which may be conceivably crystalline.) We note finally that the spectra shown in Figure 2a correspond to ice nanocrystals annealed at 140 K, a temperature just below the amorphous−cubic ice transition around 145 K; however, we verified that the 150 K spectra are similar.

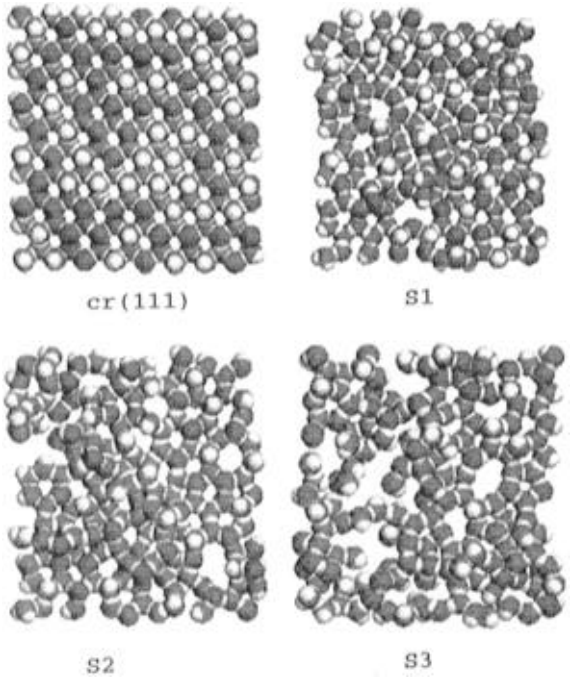

Figure 6. Topmost bilayer (160 molecules) of the model crystalline ice surface (111) and of the S1−S3 disordered surface models described in the text. Molecular graphics program: MOIL-VIEW.[30]

Simulation of all the complex processes shaping the nanocrystal surfaces is unfeasible. Even if the distribution of configurations characteristic of annealed nanocrystals is representative of thermal equilibrium, we may be unable to probe by simulation the entire range of typical configurations; this is since equilibration at low temperatures of our interest is likely to require a prohibitively large amount of computer time. We then adopted the following ad hoc approach: several (hopefully representative) ice surface structures of varying extent of disorder were generated on the computer; the different models were then used to simulate CF_4 adsorbate uptake and spectra. The objective was to find out which structural features of the surface determine the observed spectra and to try to reach useful conclusions on the nanocrystal surface structure from the comparison between the simulations and the experiments.

The procedure used to generate the ice surface models is described briefly below; more details can be found in the supporting information. In one family of models (S1−S3 in Figure 6), the starting point was a crystalline slab of six hexagonal (111) cubic ice layers. The slab (whose top layer is shown in Figure 6) was constructed by placing O atoms at perfect crystalline positions,[17] while the H atoms were distributed at random between pairs of neighboring O atoms within the well-known ice rules.[18] The linear dimensions of the model slab were $35.93 \times 38.89 \times 22$ Å. Each hexagonal layer in the crystalline model is actually a nonplanar bilayer, so that the perfect tetrahedral bonding structure is preserved. (The horizontal rows of O atoms in the crystal structure of Figure 6 alternate up and down "into the page".)

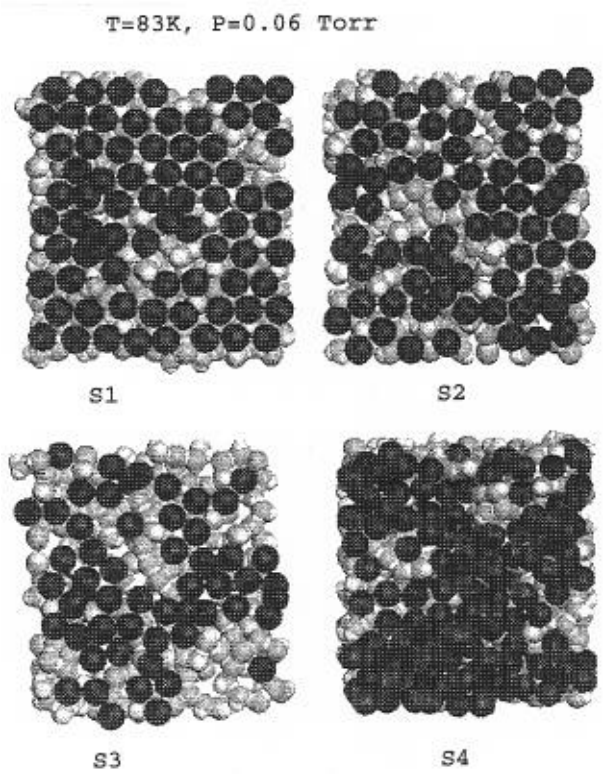

Figure 7. Snapshots of adsorbate configurations obtained in the GCMC simulations of adsorbate uptake, on model ice surfaces S1−S4, at 0.06 Torr and 83 K. CF_4 molecules are colored black, O atoms of water are gray, and H atoms of water are white.

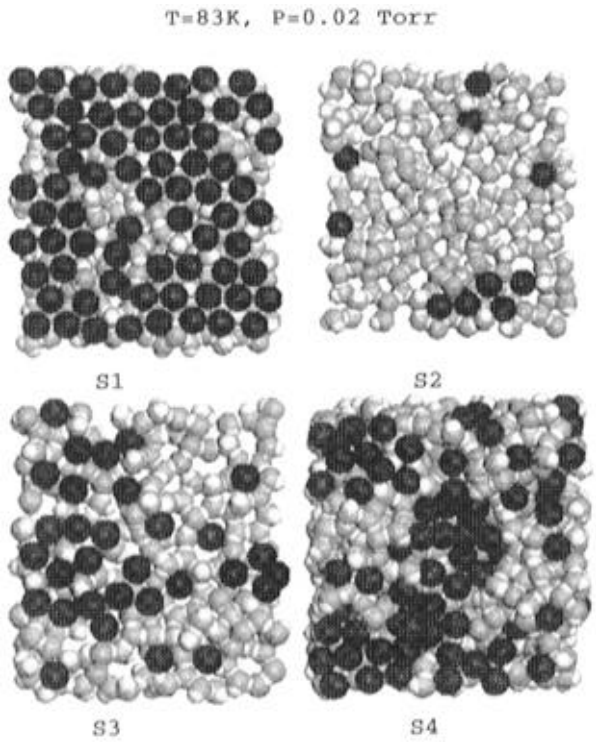

Figure 8. Snapshots of adsorbate configurations obtained in the GCMC simulations of adsorbate uptake, on model ice surfaces S1−S4, at 0.02 Torr and 83 K. CF_4 molecules are colored black, O atoms of water are gray, and H atoms of water are white.

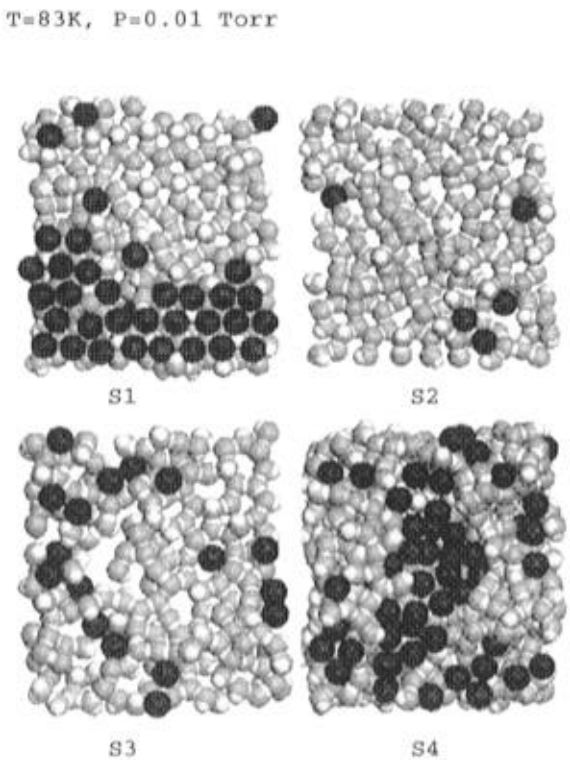

Figure 9. Snapshots of adsorbate configurations obtained in the GCMC simulations of adsorbate uptake, on model ice surfaces S1−S4, at 0.01 Torr and 83 K. CF_4 molecules are colored black, O atoms of water are gray, and H atoms of water are white.

To generate the disordered surface models S1−S3 (see Figure 6), we adopted a procedure similar to the one used in refs 4 and 8: (a) the crystal slab was heated by classical molecular dynamics (MD) to a temperature T_{max} in the range 200−250 K, (b) a classical trajectory was run at T_{max} for time t_{run} in the range 5−145 ps, to allow for structural relaxation, and (c) the resulting structure was cooled by MD to 83 K. The MD runs employed the TIPS2 potential[19] and the SHAKE rigid body algorithm.[20] The bottom two bilayers of the slab were not allowed to move. Varying extents of surface disorder were achieved by varying the values of T_{max} and t_{run}. (Since the computationally feasible rates of MD heating and cooling are orders of magnitude above the experimental, this procedure is just a computational device to generate surface models and is not designed to simulate any real physical processes.) The model S(cub) shown in Figure 10 was derived similarly from a cubic ice slab of 12 (100) ice layers. The S4 model shown in Figures 7−9 was introduced to study the effects of surface crevices and cavities; this model was generated by random removal of molecules from a surface of a (111) ice slab, followed by MD relaxation.

The S1 model, which is closest to the crystalline (111) structure (e.g., note the large percentage of hexagonal rings in the S1 structure in Figure 6), was used by us in the past to investigate ice surface spectroscopy.[4] The S1 mean potential energy is slightly lower than that of the crystal.[4] However, as described below, this model was found totally inadequate for reproducing the observed CF_4 adsorbate behavior. We still include GCMC results for CF_4 on S1 to demonstrate qualitative features of adsorbate behavior on a nearly crystalline surface. (The results are shown to be relevant to CF_4 adsorbate on CO_2 and mesitylene nanocrystals.)

Table 1 shows mean potential energies of the topmost layers of water molecules in the different models, obtained in 83 K GCMC simulations. The vertical distribution of the O atoms in the ice models was examined as well. While the slightly disordered S1 model retains a well-defined bilayer structure up to the topmost layer, in the more disordered S3 model the distribution is significantly modified and broadened in the top

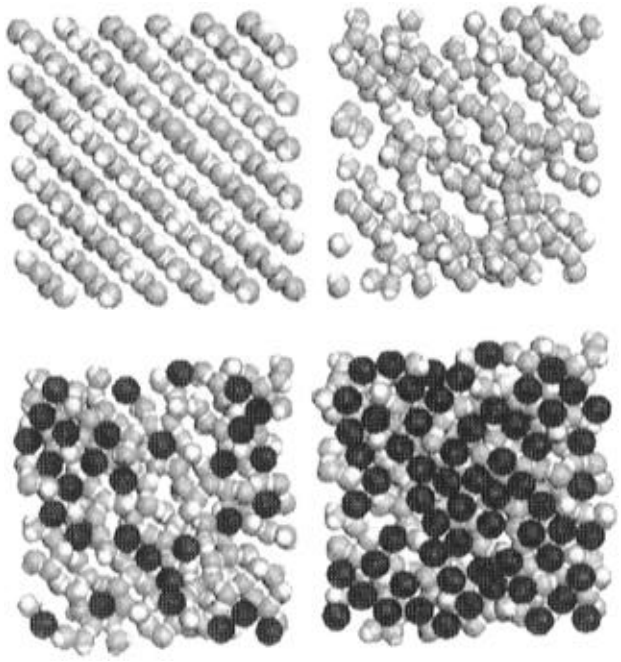

Figure 10. Top left: the topmost two layers (containing 144 molecules) of a model (100) surface of cubic ice. Top right: the relaxed S(cub) model derived from the (100) surface. Bottom panels: snapshots of adsorbate configurations on the S(cub) surface at 0.02 Torr (left) and 0.06 Torr (right).

two bilayers. In the rough S4 model, the top three bilayers are no longer well separated, while the fourth and the fifth bilayer structure is blurred. In S(cub), the vertical disorder is evident in the top four layers.

2. Grand Canonical Monte Carlo (GCMC) Simulations of CF_4 Uptake on Icy Surfaces. The description of the GCMC algorithm can be found in refs 21a−c; the version used here is described in our study[2g] of H_2 uptake on amorphous ice, with the added simplification of classical rather than quantum-mechanical treatment of the adsorbate. The objective is to obtain a collection of configurations of the adsorbate−surface system, representative of the thermal equilibrium at $T = 83$ K and a given CF_4(g) pressure. The simulation was carried out for an open μVT ensemble; the pressure of the CF_4 gas in equilibrium with the adsorbate determined the chemical potential of the adsorbate, according to the ideal gas formula. CF_4 was treated as an atom-like spherical entity. The MC steps included H_2O rotations and translations, CF_4 translations, CF_4 insertions on the surface, and CF_4 deletions. Only N_w topmost water molecules were allowed to move (see footnote of Table 1 for N_w values). The calculated CF_4 spectrum was averaged over a distribution of adsorbate configurations generated by GCMC. Further details of the GCMC procedure are given in the supporting information.

3. The Potential. The intermolecular interaction in the system was assumed to be pair additive. TIPS2[19] potential was used for water−water interaction. The $CF_4\cdots CF_4$ interaction was adopted from Sherwood and Prausnitz's analysis of the T dependence of the virial coefficients,[22] which was reproduced by them using an exp-6 potential $[\epsilon/(1 - 6/\gamma)]\{(6/\gamma)\exp[\gamma(1 - r/r_m)] - (r_m/r)^6\}$ with $\gamma = 300$, $r_m = 4.209$ Å, and $\epsilon = 403.6$ K. (The potential obtained by fitting virial coefficients is not expected to be very accurate, but at present we do not have a better source of information.) In the simulations of CF_4 uptake and spectra, the reduction of ϵ to 350 K was found to improve significantly the agreement to experiment, and this value was used in the calculations together with γ and r_m given above.

TABLE 1: Adsorbate Uptake and Energetics on Different Model Surfaces[a,b]

	P (Torr)		
	0.01	0.02	0.06
S1[b]			
E_w[c]	−5950(5)	−5948(5)	−5942(5)
N_{ads}[d]	36(3)	68(2)	76(2)
E_{tot}[e]	−1996(28)	−1987(19)	−1970(17)
$E_{ads-ice}$[f]	−1447(30)	−1351(22)	−1270(17)
$E_{ads-ads}$[g]	−550(18)	−636(14)	−701(17)
M_{per}[h]	571	544	900
S2[a]			
E_w[c]	−5933(5)	−5940(5)	−5923(4)
N_{ads}[d]	7(1)	16(4)	71(3)
E_{tot}[e]	−2223(94)	−2041(93)	−1921(19)
$E_{ads-ice}$[f]	−2163(105)	−1815(172)	−1314(30)
$E_{ads-ads}$	−60(29)	−225(108)	−607(23)
M_{per}[h]	1111	1726	1141
S3[a]			
E_w[c]	−5865(5)	−5863(5)	−5864(5)
N_{ads}[d]	15(2)	25(3)	63(4)
E_{tot}[e]	−2306(85)	−2158(52)	−1946(29)
$E_{ads-ice}$[f]	−2162(118)	−1908(86)	−1407(43)
$E_{ads-ads}$[g]	−144(45)	−250(48)	−540(43)
M_{per}[h]	559	500	1000
S4[a]			
E_w[c]	−5911(5)	−5914(4)	−5914(6)
N_{ads}[d]	52(2)	69(3)	139(4)
E_{tot}[e]	−2248(39)	−2165(52)	−2078(17)
$E_{ads-ice}$[f]	−1852(58)	−1626(42)	−1140(23)
$E_{ads-ads}$[g]	−396(28)	−539(30)	−938(21)
M_{per}[h]	658	649	900
S(cub)[a]			
E_w[c]	−5813(5)	−5813(5)	−5809(5)
N_{ads}[d]	16(3)	31(6)	62(4)
E_{tot}[e]	−2117(62)	−2003(44)	−1957(20)
$E_{ads-ice}$[f]	−1988(84)	−1753(88)	−1464(54)
$E_{ads-ads}$[g]	−129(34)	−249(63)	−493(45)
M_{per}[h]	1171	2700	1084

[a] For description of different model surfaces (S1−S4,S(cub)) see text, and figures. [b] Energies in kelvin. Numbers in parentheses are standard deviations with respect to different averaging cycles (see footnote *g* below). [c] E_w is the mean TIPS2 water−water interaction energy, per molecule, for N_w topmost molecules which are allowed to move in GCMC. For models S1−S3, $N_w = 320$ corresponds to two top bilayers; for the rough surface model S4, $N_w = 645$ includes the first (almost) complete bilayer, for S(cub) $N_w = 288$ includes the top four layers. Half of each TIPS2 pair interaction was assigned to each molecule of a pair; the sum over pair interactions includes 640 topmost molecules in models S1−S3, 1040 molecules in S4, and 864 molecules in S(cub). [d] Calculated average number of absorbate molecules. [e] Mean potential energy of adsorbate, per CF_4 molecule. [f] Mean adsorbate−surface interaction, per CF_4 molecule. [g] Mean adsorbate−adsorbate interaction, per CF_4 molecule (half of each pair interaction term was assigned to each of the two interacting molecules). [h] Number of Monte Carlo averaging cycles in a calculation; each cycle included 60 000 MC steps.

The major difficulty of the present simulation study was lack of data for the adsorbate−surface interaction. The CF_4−water interaction was modeled as an exp-6 potential function of a distance between CF_4 center and the O atom of water; the parameters were constructed by comparison to related systems of known potentials[22,23] and by final adjustment against experiment. The parameter adjustment effort was directed toward reproducing the transition from the doubly peaked CF_4 spectrum at 0.06 Torr, indicative of a continuous layer of adsorate, toward a single peak at 0.01 Torr, corresponding to isolated monomers or small groups of CF_4 at low coverages. During the adjustment, the exp-6 potential was found to give significantly better results than the Lennard-Jones function. We could not reproduce the observed behavior with any combination of parameters, if the assumed ice surface structure was the nearly crystalline S1

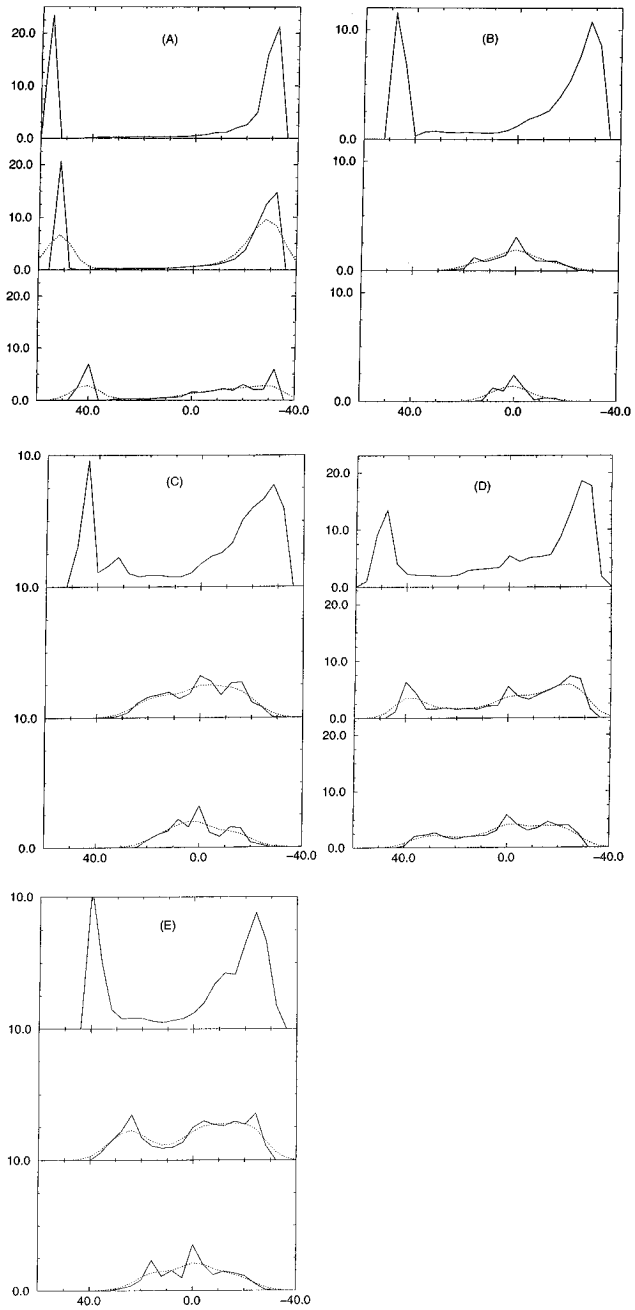

Figure 11. Simulated CF_4 adsorbate spectrum for the S1 (A), S2 (B), S3 (C), S4 (D), and S(cub) (E) ice surface models. Frequency is in cm^{-1}; the origin is set at the decoupled CF_4 frequency ($\sim$1275 cm^{-1}). CF_4 pressures from top to bottom are 0.06, 0.02, and 0.01 Torr; $T =$ 83 K. Solid, 4 cm^{-1} resolution; dotted, 10 cm^{-1} resolution. Area under the spectrum was normalized to the mean number of the of CF_4 on the surface. The computational model does not include the Evan's hole seen in the experimental spectra at 1260 cm^{-1}, which is due to resonance with a bending overtone.

model; however, reasonable qualitative agreement was obtained for the other surface models. The final parameters obtained for the exp-6 CF_4−water interaction were $\epsilon = 280$ K, $\gamma = 100$, and $r_m = 3.446$ Å.

4. GCMC Results for Adsorbate Uptake and Spectra. GCMC simulation results are now presented for the adsorbate uptake, structure, and spectra on the different ice surface models. The GCMC results are displayed in Figures 6−13 and Table 1. The simulated spectra are shown in Figure 11 for CF_4 pressures of 0.06, 0.02, and 0.01 Torr. (The low-*P* spectra are shown both at the experimental resolution of 4 cm^{-1} and smoothed over a width of 10 cm^{-1}. This is to facilitate comparison to experiment. The simulated low-*P* spectra are more structured than the experimental ones, presumably due to the small adsorbate coverage on ice models of limited size.[24])

The most interesting result of the simulations is marked sensitivity of adsorbate behavior to structural properties of the different ice surface models. From the comparison of the bare and adsorbate covered surface images (Figures 6−10), it is evident that the most relevant structural feature of the surface, with respect to the gas−surface interaction, is the ubiquitous presence of rings of water molecules on the icy surfaces; this is since interiors of such rings constitute favorable binding sites for the CF_4 adsorbate.[25] The nearly crystalline S1 surface model retained a large number of hexagonal rings characteristic of the parent (111) surface. The increasingly more disordered S2 and S3 surfaces are characterized by a significantly broader ring distribution, including much smaller and much larger rings, and a more disordered ring pattern (see Figure 6). The rough S4 surface model includes cavities in the surface, which can accommodate numerous adsorbate molecules (see, e.g., Figures 8 and 9). The S(cub) surface includes large elongated rings which are a remainder of grooves in the parent crystalline surface (Figure 10).

Adsorbate Uptake and Structure as a Function of Pressure in the S1−S4 Models; *Spectroscopic Signatures of the Different Structural Features*. Figure 7 shows the adsorbate-covered S1−S4 surfaces at 0.06 Torr. At this pressure, most of the surface is covered by adsorbate in all four models; however, there are some significant differences in the adsorbate structures. On the S1 surface, the adsorbate pattern constitutes clear evidence that this surface retained much of the hexagonal symmetry of the parent crystalline (111) surface (see Figure 6). The distribution of CF_4 coordinations[26] with respect to H_2O peaked at six, corresponding to six-coordinated sites at centers of hexagonal water rings. The distribution of CF_4 coordinations with respect to neighboring adsorbate molecules also peaks at six, corresponding to interactions of a CF_4 molecule with its CF_4 neighbors in six adjacent ring center sites. In fact, the interadsorbate lateral interactions constitute more than half of the binding energy of an adsorbate molecule to the surface. (See Table 1; in the comparison of $E_{ads-ice}$ and $E_{ads-ads}$, the latter should be multiplied by 2 since only half of each $CF_4\cdots CF_4$ interaction was assigned to each CF_4 molecule.)

As we move to the increasingly more disordered S2 and S3 surfaces, the equilibrium coverage at 0.06 Torr decreases by 7% and 17%, respectively. The reason is surface disorder. The pattern of rings is no longer ordered, and because of that the adsorbate molecules cannot acquire a full complement of six nearest adsorbate neighbors (the distribution of coordinations with respect to CF_4 peaks at five and four, respectively). The decrease in the lateral component of the adsorbate binding energy contributes to the reduction of the coverage. Moreover, the presence of the large water rings in the S2 and S3 surfaces is compensated by compact ridges of water molecules which do not include rings large enough to provide low-energy binding sites for CF_4, and these regions are visible in Figure 7 as bare portions of the S2 and S3 surfaces. The uptake increases again, by about a factor of 2, on the very rough S4 surface with crevices. Here CF_4 adsorption is three-dimensional rather than two-dimensional. The contribution of interadsorbate interactions to adsorbate bonding is even larger than in the S1 case; the distribution of the adsorbate coordinations with respect to CF_4 peaks at eight, while the distribution of coordinations with respect to water is very broad and extends from 0 to 15. In the S4 model, the vertical width of the adsorbate distribution at

0.06 Torr (i.e., the width of the CF_4 *z*-distribution) is about 8.25 Å, as compared to 0.75, 1.75, 2.25, and 2.75 Å in models S1−S3 and S(cub), respectively.

One should emphasize the broader range of adsorbate bonding possibilities in the disordered S2−S4 models, as compared to the nearly crystalline S1 model. While the structure of the S1 surface allows for simultaneously high 6-fold coordination of CF_4 with respect to both H_2O and the adsorbate neighbors, the adsorbate layer in S2−S4 models includes molecules of low coordination with respect to CF_4, which is compensated by high coordination with respect to H_2O, and vice versa. The first category corresponds to CF_4 in deep surface sites, which can be found inside large H_2O rings or cavities, and the second category to CF_4 on "ridges" of water molecules, with neighboring adsorbate molecules supplying much of the binding energy.

While all the simulated spectra display at 0.06 Torr the LO−TO doublet with the LO peak narrower than the TO (see Figures 11A−D), there are significant differences between the four spectra. The LO−TO splitting is 88/76/72/78 cm^{-1} for models S1−S4, respectively. Not unexpectedly, the splitting is largest for the nearly crystalline S1 model; moreover, the TO peak in S1 is markedly narrower than in the remaining models, and the absorption intensity in the region intermediate between the LO and the TO is smallest. The decrease in the splitting in the sequence S1−S2−3 is due to the reduced coverage and the increase in the surface disorder (see Figure 7 and Table 1). The larger splitting in S4 as compared to either S2 or S3 is probably due to much larger adsorbate coverage. In models S1−S3 the LO peak height is somewhat larger than that of the TO, as expected for CF_4 on smooth but laterally disordered surfaces (see section IIIB2). In model S4, surface roughness is sufficient to broaden LO to the extent that the peak height order is reversed.

The difference in adsorbate behavior between the four S1−S4 models is even larger as the CF_4 pressure is lowered from 0.06 to 0.02 and 0.01 Torr (see Figures 7−9 and Table 1). On the S1 surface, almost full monolayer is retained at 0.02 Torr; at 0.01 Torr the coverage drops by about a factor of 2, but strong lateral interactions still hold the CF_4 molecules together in an extended patch in which the hexagonal pattern is still apparent. Because of that, a well-developed LO−TO doublet corresponding to collective vibrations of the adsorbate is present in the simulated spectra down to 0.01 Torr (see Figure 11A).

In contrast to that, on a disordered surface S2, the coverage drops dramatically by a factor of 4 and 10 at 0.02 and 0.01 Torr, respectively; at 0.01 Torr the mean coverage is only a few molecules. The difference with respect to the S1 surface is explained by weakening of the interadsorbate interactions due to disorder, as explained above. The molecules remaining on the S2 surface are found in a few deep sites in particularly large water rings that are present on the surface; these adsorbate molecules appear either as monomers or in small groups. Accordingly, the simulated spectra at 0.02 and 0.01 Torr correspond to relatively narrow peaks (fwhm of ∼24 and ∼17 cm^{-1} at 0.02 and 0.01 Torr, respectively; see Figure 11B).

On the even more disordered S3 surface, the low-*P* coverage *increases* by a factor of 1.6−2 with respect to S2. The reason is the presence of even larger rings on S3, which can accommodate more than one CF_4 molecule. Some of these rings are close to each other, which at 0.02 Torr results in the coexistence of extended groups both of CF_4 and of CF_4 monomers (see Figures 8 and 9). As a result, the low-*P* spectral bands are significantly broader than in the case of S2 (fwhm of ∼45 and ∼32 cm^{-1} at 0.02 and 0.01 Torr, respectively; see Figure 11C).

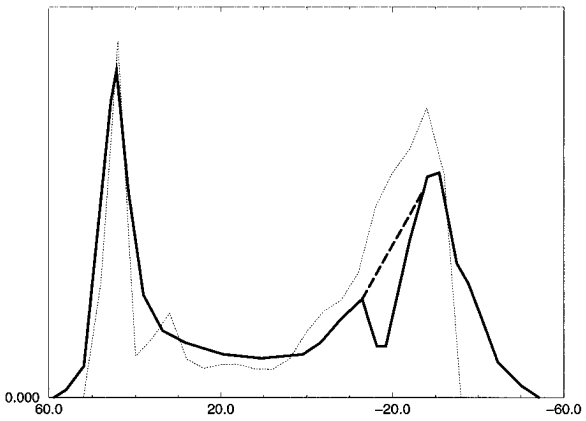

Figure 12. Simulated CF_4 spectrum obtained in model S3 at 0.06 Torr and 83 K (dotted), compared to the experimental spectrum on annealed nanocrystals (solid, 0.06 Torr spectrum from Figure 2a). The two spectra were normalized to the same integrated intensity. The edges of the Evan's hole, which was not included in the computational model, are connected in the experimental spectrum by the dashed line, to facilitate visual comparison.

On the rough S4 surface, the low-*P* uptake of adsorbate is much larger than on either S2 or S3; the adsorbate is found in "pools" which occupy the crevices in the surface (see Figures 8 and 9). The presence of such extended "pools" results in the relatively large width of the low-*P* simulated spectra (66 and 60 cm^{-1} at 0.02 and 0.01 Torr, respectively; see Figure 11D). Roughly, the low-*P* spectra look like a superposition of the LO−TO split contribution from the pools and a contribution near zero frequency from monomers and small groups of adsorbate present outside the crevices.

In the comparison with experiment, we focus on the annealed nanocrystal spectra shown in Figure 2a. At 0.06 Torr, the experimental spectrum displays a well-developed LO−TO doublet, split by 73 cm^{-1}. At 0.02 Torr the doublet collapses into a broad flat peak with some residual LO−TO structure at the edges, split by ∼50 cm^{-1}. At 0.01 Torr a single peak is present, of fwhm of about 50 cm^{-1}. Perhaps the best overall qualitative agreement with experiment is obtained with the disordered S3 model (see Figures 2a, 11, and 12). The crystalline S1 model yields a well-developed LO−TO doublet down to 0.01 Torr, in disagreement with experiment. The disordered S2 model yields low-*P* spectra which are too narrow, while the low-*P* spectra of S4 are too broad.

The S(cub) Surface: Adsorbate Uptake and Spectra. The interesting feature of the results for this surface is their qualitative similarity to the results for the S3 surface (see Figure 11 and Table 1). This is despite the fact that the two models were derived from different crystallographic surfaces and are quite different structurally (compare Figure 6 with Figure 10). In the S(cub) model, the large rings are oriented preferentially along the diagonal, while in S3 no such preferential orientation of large rings is apparent. The radial distribution functions of CF_4 obtained on the two surfaces at 0.06 Torr (not shown) are also quite different from each other. However, the spectra of the CF_4 adsorbate on the two surfaces are qualitatively quite similar to each other. (Compare parts C and E of Figure 11; in S(cub) the 0.06 Torr LO/TO splitting is lower by 8 cm^{-1} than in S3, but the bandwidths at 0.02 and 0.01 Torr are larger by several cm^{-1}.) It is then seen that the characteristic "broad TO/narrow LO" spectral signature of a thin laterally disordered CF_4 monolayer can be obtained on disordered surfaces of markedly different molecular structures. The microscopic surface property which is shared by both S3 and S(cub) models and which causes the broad 0.02 Torr spectrum is the presence of larger water

rings, of size sufficient to accommodate a few CF_4 molecules each (see Figures 8 and 10).

IV. Discussion

In this section the experimental results are interpreted, using the results of the simulations. The emphasis is on the question: what can one learn about the *nanocrystal surface* from simulated versus experimental spectra of CF_4 adsorbate?

We first consider surfaces of the annealed ice nanocrystals. Simulations suggest that the surfaces of the annealed nanocrystals are smooth but laterally disordered and include some large rings of water molecules (large enough to accommodate a few CF_4 molecules). Smooth but laterally disordered surface structure is inferred from the "sharp LO/broad TO" spectral pattern obtained experimentally at 0.06 Torr (see Figure 2a), which can be reproduced qualitatively by calculations of spectra of random CF_4 layers of thickness below 3 Å (see Figure 5b). A spectral pattern similar to experiment was also obtained in GCMC simulations of CF_4 adsorbate on the S3 and S(cub) ice surface models at $P = 0.06$ Torr (see Figures 2a, 11C,E, and 12). The S3 and S(cub) models are both disordered but structurally different from each other (see Figures 6 and 10); they were constructed by "relaxing" two different crystalline faces of cubic ice as described in section IIIC1. A surface of a nanocrystal is likely to include structurally different patches related to different crystalline faces of ice. Numerical experiments of section IIIB suggest, however, that the spectral signature of a thin laterally disordered CF_4 layer ("sharp LO/broad TO") allows for considerable inhomogeneity in the structure of the adsorbate layer and of the underlying surface.

The presence of large rings of water molecules in the structure of the annealed nanocrystal surfaces is suggested by the broad flat spectrum obtained experimentally at 0.02 Torr (see Figure 2a) and reproduced qualitatively in GCMC simulations on the S3 and S(cub) models. In these models, the presence of large rings which can accommodate several CF_4 molecules results in the presence of extended groups of CF_4 adsorbate on the surface and therefore in considerable width of the 0.02 Torr spectrum. A continuous broad spectrum (rather than a well-separated LO−TO doublet) is obtained at this pressure due to a *distribution* of sizes of CF_4 adsorbate groups, which extends down to monomers. The low-*P* line widths place constraints on large water ring structures or cavities present in the annealed nanocrystal surfaces. Thus, the ring distribution of the experimental annealed nanocrystal surfaces may be even broader than the one in our finite size S3 and S(cub) models, since the simulated low-*P* spectra are narrower than the experimental ones. On the other hand, the S4 model with large crevices (which can accommodate a much larger amount of adsorbate than the large rings in S3 and S(cub), see Figures 8 and 9 and Table 1) yields low-*P* spectra that are broader than the experimental ones.

The level of agreement with experiment attained in the present calculations is qualitative rather than quantitative, which is not surprising considering the various uncertainties and approximations of the computational scheme (see sections IIIA and IIIC1,3). Figure 12 shows comparison between the experimental spectrum of CF_4 on the annealed nanocrystals at 0.06 Torr and the spectrum calculated for the adsorbate on the S3 surface model. In addition to the absence of the Evan's hole at 1260 cm^{-1} (which was not included in the computational scheme), the major discrepancy is the too abrupt decrease of the calculated TO peak toward the low frequencies. Comparison of random shell and random layer results in Figure 5b suggests that the discrepancy may be due to neglection of surface curvature in the S3 model.

The calculated relative uptake of CF_4 was compared to the experimental one for the annealed nanocrystals, as follows. A rough estimate for the experimental uptake was obtained by estimating the area under the CF_4 absorption spectrum, using a standard computer software (Jandel's "Peakfit"); the relative uptake at 0.01/0.02/0.06 Torr was found to be 0.18/0.32/1, respectively. These values can be compared to the calculated ones (see Table 1) of 0.47/0.89/1 for the S1 model, 0.10/0.25/1 for S2, 0.28/0.40/1 for S3, 0.37/0.50/1 for S4, and 0.26/0.50/1 for S(cub). The estimated experimental values are below the results for S3 and S(cub) and above S2; the results for both the very rough S4 model and the smooth nearly crystalline S1 model are too high.

Additional experimental support for the proposed lateral disorder of the annealed ice nanocrystal surfaces comes from the similarity of the CF_4 adsorbate spectra obtained experimentally on their surfaces to the CF_4 spectra obtained on some glassy molecular nanoparticles. As an example, Figure 4a shows CF_4 spectra measured on amorphous mesitylene nanoparticles. In this case, the nanoparticle interior is glassy, and therefore the surface is expected to be disordered as well. The evolution of the spectrum from the "broad TO/narrow LO" pattern (with LO peak intensity larger than that of TO), to a broad flat spectral feature, and then to a single peak as the coverage is decreased is similar to the evolution of the CF_4 adsorbate spectra on ice as seen in Figure 2a. (The pressure range in which this evolution occurs is different in the two adsorbate−surface systems, since the binding energy of CF_4 on mesitylene is lower than on ice.) A qualitatively similar spectral pattern was also observed on glassy methanol nanoparticles.

While the simulated spectral patterns obtained for ordered and nearly ordered CF_4 layers are in clear disagreement with experiment on ice nanocrystals, they match the qualitative behavior obtained experimentally on mesitylene and CO_2 nanocrystals. Thus, the latter nanocrystals seem to have crystalline interiors *and* surfaces. At 0.08−0.1 Torr (presumably close to a monolayer coverage) the LO and TO peaks on crystalline mesitylene have similar widths, and the TO peak intensity is larger than that of the LO (Figure 4b). This in contrast to the glassy mesitylene surface (Figure 4a), on which the TO peak is broader than the LO and the order of the peak heights is reversed. These results are in accord with spectral patterns computed for ordered versus laterally disordered CF_4 layers in section IIIB (compare parts a and b of Figure 5). Thus, the CF_4 monolayer on crystalline mesitylene appears to be ordered, suggesting crystallinity of the underlying surface.

Comparison of CF_4 spectra measured on crystalline mesitylene to GCMC simulation results on the nearly crystalline S1 ice surface model is also of interest (compare Figure 4b to Figure 11A). On the S1 surface, the disorder in the CF_4 monolayer structure is sufficient to make peak intensities of LO and TO approximately equal[14] (see Figure 7). However, another striking result obtained in this model is also valid for the experimental spectra on crystalline mesitylene; this is the retention of the doublet spectral pattern characteristic of extended groups of adsorbate down to the lowest pressures and submonolayer coverages. According to the simulations, on the smooth homogeneous crystalline surfaces the strong lateral interactions keep adsorbate molecules together down to low pressures. This is in contrast ot the glassy surfaces, on which the adsorbate spectrum collapses to a single peak as *P* is lowered, due to the dominant presence of isolated CF_4 monomers and small CF_4 groups. The latter occupy deepest sites available in the inhomogeneous surface.

Spectral patterns characteristic of ordered adsorbate were also obtained experimentally for CF_4 on CO_2 nanocrystals (see Figure 4c). This result is not unexpected, since, as argued in section IIIC1, the surfaces of CO_2 nanocrystals are *expected* to be crystalline. One may note that the low-*P* spectra of CF_4 on crystalline surfaces contain information on the shape of the adsorbate patches remaining at low pressures. The "inverted" LO−TO splitting pattern measured for mesitylene at the lowest *P* (see Figure 4b) suggests linear patterns of CF_4 adsorbate,[12a,b] while the low-pressure spectrum on CO_2 (Figure 4c) is closer to that of the S1 model at 0.01 Torr and is consistent with roughly square and/or rectangular CF_4 patches (see the S1 panel in Figures 9 and 11A).

We now consider the surface structure of the unannealed ice nanocrystals as inferred from the experimental CF_4 adsorbate spectra shown in Figures 2b and 3a. The differences of the 0.06 Torr spectra with respect to the annealed nanocrystal spectra shown in Figure 2a include broadening of both the LO and the TO peaks, reduction of the LO−TO splitting from 73 cm^{-1} (for the 140 K anneal) to 68 cm^{-1} (unannealed nanocrystals, large cell) and 50 cm^{-1} (unannealed, small cell), TO maximum intensity larger than the LO one, and significant enhancement of the intensity between the two peaks. According to simulations of random CF_4 layers described in section IIIB, these changes suggest that the surface of unannealed ice nanocrystals is both disordered and very rough.

Model S4 described in section IIIC1,4 was constructed by removing molecules at random from the (111) surface, in an effort to obtain a molecular structure for such a rough ice surface; this model proved to be much less successful than model S3 for the annealed nanocrystals. At 0.06 Torr, the calculated TO−LO splitting is too large (78 cm^{-1}); at 0.01 Torr, the simulated spectrum is too broad. It appears that the S4 surface is still too smooth and/or too ordered to be representative of unannealed nanocrystals.

It is likely that the surface texture of the unannealed nanocrystals (at least the small cell ones) is similar to that of the vapor-deposited microporous amorphous ice;[2k,27] the evidence is the qualitative similarity between the experimentally measured CF_4 spectra on the two surfaces, as seen in Figure 3a,b, together with the "amorphous" component of the HOD spectra of the unannealed small cell nanocrystals (see Figure 1b and section IIB1). The main difference between the spectra in Figure 3a,b is the residual LO−TO structure present in the 0.06 Torr adsorbate spectrum on the unannealed clusters, while the spectrum on amorphous ice is almost flat.

To model the amorphous ice surface structure and its interaction with adsorbates, we have used in the past an amorphous cluster model $(H_2O)_{450}$ generated by simulated condensation of water vapor.[6] This model, covered by a simulated CF_4 layer at 0.06 Torr and 83 K, is shown in Figure 13. In contrast to the S4 surface model (on which the GCMC simulation yielded a nearly continuous adsorbate layer, see Figure 7), the adsorbate structure on the rough and disordered amorphous cluster surface is characterized by isolated CF_4 "pools" in surface crevices and indentations. The simulated CF_4 spectrum shown in Figure 13 is somewhat narrower (fwhm $\sim$ 45 cm^{-1}) than the one obtained experimentally for CF_4 on unannealed small cell nanocrystals (Figure 3a), and the residual LO−TO pattern is not visible. This discrepancy can be accounted for by an order of magnitude difference between the size of the simulated cluster (a few nanometers) and the typical size of the nanocrystals (see Figure 5d and the end of section IIIB).

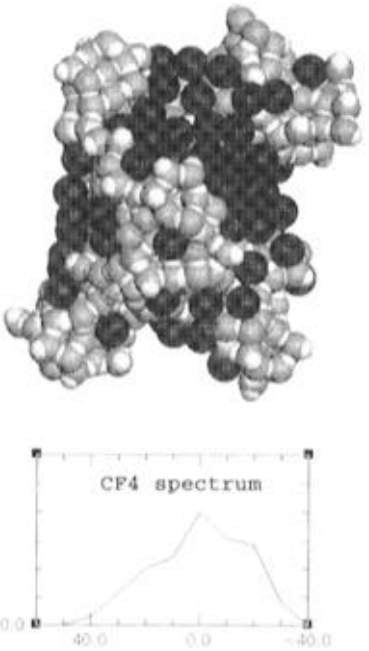

Figure 13. Image of CF_4 adsorbate on a model amorphous ice cluster; a snapshot from a GCMC simulation at 0.06 Torr and 83 K. Inset: a simulated CF_4 spectrum, with a resolution of 10 cm^{-1}.

The flatness of the experimental spectrum of CF_4 on amorphous ice at 0.06 Torr is somewhat puzzling. The diameter of the micropores of amorphous ice was estimated[27] to be $\lesssim$2 nm, similar to the linear dimension of the model cluster. Thus, if the texture of the model cluster is in fact representative of the micropore surface, the cluster model can be viewed as an "inverted micropore", and the size difference cannot account for the difference between the calculated and the experimental line shape. Perhaps the micropores form elongated channels oriented preferentially in the direction perpendicular to the amorphous ice film; then the radiation (whose electric vector is parallel to the film) would have enhanced probability for normal or nearly normal orientation with respect to the micropore surface. The high-frequency "LO-like" region would then be enhanced with respect to the low-frequency TO region. Simulations of ellipsoid CF_4 shells confirm that elongation in fact produces this effect.

V. Summary and Concluding Remarks

This study focuses on spectroscopy of CF_4 adsorbed on ice nanocrystals. Due to strong intermolecular dipole−dipole coupling, the asymmetric CF stretch excitations tend to be collective and structure sensitive (especially sensitive to the extent of surface disorder). We then use comparison between theory and experiment to try to reach useful conclusions on the structure of the adsorbate layer and of the underlying ice surface of the nanocrystals. Spectra were calculated for various simple *assumed* structures of the adsorbate layer, both ordered and disordered. Furthermore, several microscopic models of varying extent of disorder were constructed for the ice surface and used in grand canonical Monte Carlo simulations of CF_4 adsorbate uptake, structure, and spectra. Comparison of calculations to experiment suggests that unannealed ice nanocrystal surfaces are disordered and very rough and that the surfaces of annealed nanocrystals are relatively smooth but still laterally disordered. The structural feature which is found to be most significant for the CF_4 adsorbate uptake on annealed icy surfaces is a ubiquitous presence of rings of water molecules in the surface, since such rings provide favorable binding sites for the CF_4.[25] Present

results suggest a broad ring size distribution in the annealed ice surface, including rings large enough to accommodate several CF_4 molecules. Such large rings are likely to provide favorable sites for the extensively studied acid ionization on icy surfaces (e.g., refs 1a−c, 2h, 28, and 29).

Laterally disordered surface structure seems to be thermodynamically (rather than kinetically) favored by the annealed ice nanocrystals; this is since annealing at 140−150 K shoud be sufficient to induce relaxation to a crystalline surface form, if the lattter were more favorable (see section IIIC1). Disorder in the ice surface structure was already suggested in some past studies,[4,8] in which it was proposed to be driven by formation of hydrogen bonds between dangling atoms of surface H_2O molecules, at the expense of the lateral order. Additional (entropic) contribution to disorder may be due to enhanced freedom of motion of surface water molecules, which may allow them to probe a broad range or nonperiodic configurations.

It should be noted that the CF_4 line shape on annealed H_2O nanocrystals is similar to that obtained experimentally on glassy mesitylene whose surface is almost certainly disordered. On the other hand, CF_4 adsorate spectra on CO_2 and mesitylene nanocrystals match patterns calculated for crystalline or nearly crystalline surfaces. Thus, the CF_4 adsorbate spectroscopy is suggested here as a useful tool for characterization of surface properties of molecular solids and of large molecular clusters.

Acknowledgment. V.B. and J.P.D. acknowledge the support of BSF Grant CHE-9022055 and of the NSF Grant CHE-9319176. C. Simmerling is acknowledged for making available his molecular graphics program, MOIL-VIEW.[30] We thank T. Feldmann and E. Gershgoren for providing very helpful models of ice structure. Helpful discussions are acknowledged with A. Ben-Shaul, C. A. Wight, and G. Torchet.

Supporting Information Available: Detailed description of ordered and random layer models used in section IIIB, procedures for generation of ice surface models S1−S4, and GCMC algorithm (7 pages). Ordering information is given on any current masthead page.

References and Notes

(1) For example: (a) Molina, M. J.; Tso, T. L.; Molina, L. T.; Wang, F. C. Y. *Science* **1987**, *238*, 1253. (b) McCoustra, M. R. S.; Horn, A. B. *Chem. Soc. Rev.* **1994**, *23*, 195. (c) Tolbert, M. A.; Rossi, M. J.; Malhorta, R.; Golden, D. M. *Science* **1987**, *238*, 1258. (d) Tielens, A. G. G. M.; Allamandola, L. J. In *Physical Processes in Interstellar Clouds*; Morfill, G. E., Scholet, M., Eds.; Reidel: Dordrecht, 1987. (e) Buch, V. In *Molecular Astrophysics*; Hartquist, W. T., Ed.; Cambridge University: Cambridge, 1990.

(2) For example: (a) Rowland, B.; Fisher, M.; Devlin, J. P. *J. Chem. Phys.* **1991**, *95*, 1378. (b) Buch, V.; Devlin, J. P. *J. Chem. Phys.* **1991**, *94*, 4091. (c) Buch, V.; Czerminski, R. *J. Chem. Phys.* **1991**, *95*, 6026. (d) Devlin, J. P. In *Physics and Chemistry of Ice*; Maeno, N., Hondoh, T., Eds.; Hokkaido University: Sapporo, 1992. (e) Devlin, J. P. *J. Phys. Chem.* **1992**, *96*, 6185. (f) Hixson, H. G.; Wojcik, M. J.; Devlin, M. S.; Devlin, J. P.; Buch, V. *J. Chem. Phys.* **1992**, *97*, 753. (g) Buch, V.; Devlin, J. P. *J. Chem. Phys.* **1993**, *98*, 4195. (h) Delzeit, L.; Rowland, B.; Devlin, J. P. *J. Phys. Chem.* **1993**, *97*, 10312. (i) Devlin, J. P.; Silva, S. C.; Rowland, B.; Buch, V. In *Hydrogen Bond Networks*; Belissent-Funel, M. C., Dore, J. C., Eds.; Kluwer: Netherlands, 1994. (k) Devlin, J. P. *Int. Rev. Phys. Chem.* **1990**, *9*, 29. (j) Sadlej, J.; Rowland, B.; Devlin, J. P.; Feldmann, T.; Buch, V. *J. Chem. Phys.* **1995**, *102*, 4804.

(3) Devlin, J. P.; Buch, V. *J. Phys. Chem.* **1995**, *99*, 16534.

(4) Rowland, B.; Kadagathur, N. S.; Devlin, J. P.; Buch, V.; Feldmann, T.; Wojcik, M. J. *J. Chem. Phys.* **1995**, *102*, 8328.

(5) Rowland, B.; Kadagathur, N. S.; Devlin, J. P. *J. Chem. Phys.* **1995**, *102*, 13.

(6) Buch, V. *J. Chem. Phys.* **1992**, *96*, 3814. In the present GCMC simulations, the amorphous cluster temperature was adjusted by MD to 83 K.

(7) Materer, N.; Starke, U.; Barbieri, A.; van Hove, M. A.; Somorjay, G. A.; Kroes, G. J.; Minot, C. *J. Phys. Chem.* **1995**, *99*, 6267.

(8) Kroes, G. J. *Surf. Sci.* **1992**, *275*, 365.

(9) Karim, O. A.; Haymet, A. D. J. *J. Chem. Phys.* **1988**, *89*, 6889.

(10) For example, Thiel, P. A.; Madey, T. E. *Surf. Sci. Rep.* **1987**, *17*, 211. Pirug, G.; Ritke, C.; Bonzel, H. P. *Surf. Sci.* **1991**, *241*, 289. Schaff, J. E.; Roberts, J. T. *J. Phys. Chem.* **1994**, *98*, 6900. Held, G.; Mentzel, D. *Surf. Sci.* **1995**, *327*, 301. Livneh, T.; Roman, L.; Asscher, M. Preprint. Xinfu, X.; Berkowitz, M. L. *Phys. Rev. Lett.* **1995**, *74*, 3193.

(11) Jones, L.; Swanson, B. I. *J. Phys. Chem.* **1991**, *95*, 2701.

(12) General discussion of LO−TO splitting in molecular solids can be found in: (a) Decius, J. C.; Hexter, R. M. *Molecular Vibrations in Crystals*; McGraw-Hill: New York, 1977. (b) Califano, S.; Schettino, V.; Neto, N. *Lattice Dynamics of Molecular Crystals*; Springer: Berlin, 1981. LO−TO splitting for multilayers of molecular adsorbates on NaCl is discussed by: (c) Chang, H. C.; Richardson, H. H.; Exing, G. E. *J. Chem. Phys.* **1988**, *89*, 7561. (d) Berg, O.; Ewing, G. E. *Surf. Sci.* **1989**, *220*, 198. Recent studies of effects of dipole−dipole coupling on infrared spectra of crystalline and amorphous thin films include: (e) Ovchinnikov, M. A.; Wight, C. A. *J. Chem. Phys.* **1994**, *100*, 972. (f) Ovchinnikov, M. A.; Wight, C. A. *J. Chem. Phys.* **1995**, *102*, 67.

(13) Person, W. B.; Zerbi, G. *Vibrational Intensities in Infrared and Raman Spectroscopy*; Elsavier: New York, 1982; Chapter 14.

(14) It should be emphasized that the transition from the "crystalline" pattern seen in Figure 5a to the "broad TO/narrow LO" pattern seen in Figure 5b is due predominantly to the lateral disorder. If the width of the vertical distribution for the crystalline cubic structure is increased to 2.5 Å, there is some broadening in TO, and the maximum intensities of the TO and the LO peaks become equal; however, the resulting TO line width is ∼3 times smaller than that in the solid spectrum in Figure 5b.

(15) Torchet, G.; Schwartz, P.; de Feraudy, M. F.; Raoult, B. *J. Chem. Phys.* **1983**, *79*, 6196. Torchet, G.; Farges, J.; de Feraudy, M. F.; Raoult, B. *Ann. Phys. Fr.* **1989**, *14*, 245.

(16) (a) Huang, J.; Bartell, L. S. *J. Phys. Chem.* **1994**, *98*, 7455. (b) Huang, J.; Bartell, L. S. *J. Phys. Chem.* **1995**, *99*, 3924.

(17) Eisenberg, D.; Kautzmann, W. *The Structure and Properties of Water*; Oxford University: Oxford, 1969.

(18) Bernal, J. D.; Fowler, R. H. *J. Chem. Phys.* **1933**, *1*, 515. Pauling, L. *J. Am. Chem. Soc.* **1935**, *57*, 2680.

(19) Jorgensen, W. L. *J. Chem. Phys.* **1982**, *77*, 4156. Jorgensen, W. L.; Chandrasekhar, J.; Madura, J. D.; Impey, R. W.; Klein, M. L. *J. Chem. Phys.* **1983**, *79*, 926.

(20) Ryckart, J. P.; Ciccotti, G.; Berendsen, H. J. C. *J. Comput. Phys.* **1977**, *23*, 327.

(21) (a) Norman, G. E.; Filinov, V. S. *High Temp. (USSR)* **1969**, *7*, 216. (b) Adams, D. J. *Mol. Phys.* **1974**, *28*, 1241; **1975**, *29*, 307. (c) Valleau, J. P.; Cohen, L. K. *J. Chem. Phys.* **1980**, *72*, 5935.

(22) Sherwood, A. E.; Prausnitz, J. M. *J. Chem. Phys.* **1964**, *41*, 429.

(23) Becker, C. H.; Tiedemann, P. W.; Valentini, J. J.; Lee, Y. T.; Walker, R. B. *J. Chem. Phys.* **1979**, *71*, 481.

(24) Moreover, the only source of line broadening included in the calculations is the dipole−dipole coupling, while in reality an additional broadening contribution is probably present due to a distribution of local adsorbate environments. The latter contribution should be particularly significant at low pressures at which the mean interadsorbate interaction is reduced and the mean gas−surface interaction increased.

(25) Water molecule rings as favorable binding sites for adsorbate have been noted in the past in MD simulations of HCl and ClOH sticking on the (0001) surface of hexagonal ice by: Kroes, G. J.; Clary, D. C. *J. Phys. Chem.* **1992**, *96*, 7079.

(26) Coordination of a CF_4 molecule with respect to H_2O was defined using a cutoff distance of $r(CF_4\cdots O) = 4.75$ Å; coordination of CF_4 with respect to other CF_4 was defined using a cutoff of $r(CF_4\cdots CF_4) = 5.75$ Å. These cutoffs were extracted as the end points of the nearest-neighbor peaks in the respective radial distribution functions.

(27) Meyer, E.; Pletzer, R. *J. Phys., Colloq.* **1987**, *48*, C1−581; *Nature* **1986**, *319*, 298.

(28) Robertson, S. H.; Kroes, G. J.; Clary, D. C. *Faraday Discuss.*, to be published.

(29) Koehler, B. J.; Middlebrook, A. M.; McNeil, L. S.; Tolbert, M. A. *J. Geophys. Res.* **1993**, *88*, 10563. Koehler, B. J.; Middlebrook, A. M.; McNeil, L. S.; Tolbert, M. A. *J. Geophys. Res.* **1993**, *88*, 10563.

(30) Simmerling, C.; Elber, R.; Zhang, J. In *Modelling of Biomolecular Structures and Mechanisms*; Pullman, A., Ed.; Kluwer: Dordrecht, 1995; pp 241−265.

JP952193W